V. N. Bas International Journal of Applied Pharmaceutics

ISSN- 0975-7058 Vol 18, Issue 3, 2026

Original Article

INTEGRATED BIOANALYTICAL METHOD VALIDATION, PHARMACOKINETICS, AND METABOLITE CHARACTERIZATION OF 19-MONOAMINOTHIAZOLE (19MAT): A CORRELATIVE *IN-SILICO* AND *IN VIVO* STUDY USING LC–MS/MS

VINAY N. BASAVANAKATTI[1], MOHAMMAD ALI[1*], SHEIKH MURTUJA[2,3], BARIJ NAYAN SINHA[2], VENKATESAN JAYAPRAKASH[2]

[1]Department of Pharmacology, Faculty of Pharmacy, Sri Adichunchanagiri College of Pharmacy, Adichunchanagiri University, B. G. Nagara-571448, Mandya District, Karnataka, India. [2]Department of Pharmaceutical Sciences and Technology, Birla Institute of Technology, Mesra, Ranchi-835215, Jharkhand, India. [3]Department of Pharmaceutical Technology, School of Health and Medical Sciences Adamas University, Kolkata-700126, West Bengal, India

[*]Corresponding author: Mohammad Ali; [*]Email: alimohammad973@gmail.com

Received: 13 Jan 2026, Revised and Accepted: 02 Mar 2026

ABSTRACT

Objective: This study is mainly focused on the development and validation of a robust liquid chromatography–tandem mass spectrometry (LC–MS/MS) method to accurately evaluate the pharmacokinetics (PK) and metabolite profile of 19-Monoaminothiazole (19MAT), a newly synthesized compound showing promising antiviral activity against dengue virus (DENV). The work additionally integrated *in silico* metabolite prediction tools with experimental *in vivo* metabolite identification data to comprehensively understand the metabolic fate of 19MAT.

Methods: Triple-quadrupole LC–MS/MS method was developed and validated as per ICH M10 (International council for harmonization of technical requirements for pharmaceuticals for human use) guidelines for its selectivity, linearity (1.27–1270 ng/ml), accuracy/precision, recovery, matrix effect, stability in rat plasma to quantify 19MAT to assess the PK after IV (Intravenous) and PO (Per oral) administration. Waters Xterra RP® C_{18} (150 mm × 4.6 mm, 5 µm) column was used in reverse phase separation of analyte and internal standard. Pharmacokinetics was assessed in Sprague Dawley rats (n=3 per dose group). BioTransformer 3.0 and SMARTCyp3.0 were used to predict metabolites, and a targeted LC–MS/MS strategy was used to identify the metabolites in plasma, urine, and feces.

Results: The assay showed linear response with r^2>0.99, recovery 48–63% with acceptable matrix factors, precision ≤~11% RSD (Relative standard deviation), and stability up to 45 days (−20/−70 °C). 19MAT exhibited rapid oral absorption (T_{max} ≈ 0.42 h), moderate half-life (PO: 4.20 h), high V_d (IV: ~1977 ml/kg), and bioavailability of 23.82%. Seven metabolites were identified via plasma, urine, and feces involving hydroxylation/dihydroxylation, O-dealkylation, and glucuronidation.

Conclusion: The integrated workflow establishes validated quantitation approach, appropriately identified pharmacokinetic properties, and maps metabolic pathways for 19MAT, supporting preclinical optimization.

Keywords: LC-MS/MS, Pharmacokinetics, 19MAT, *In silico*, Biotransformer 3.0, SMARTCyp 3.0, Metabolite identification and Absolute bioavailability

DOI: https://dx.doi.org/10.22159/ijap.2026v18i3.58083 Journal homepage: https://innovareacademics.in/journals/index.php/ijap

INTRODUCTION

Thiazole and aminothiazole heterocyclic scaffolds are two classes that are often used as new chemical entities (NCEs) due to their pharmacophoric versatility and documented antiviral potentials across multiple viral families. These scaffolds are likely to have metabolic problems, such as breaking down quickly in oxidative environments, opening their rings, and making intermediates that could be reactive. These problems have made it even more important to include drug metabolism and pharmacokinetics (DMPK) properties early in the drug discovery and development stage to improve the efficiency of antiviral discovery programs and reduce attrition at later stage [1-3].

Thiazole and aminothiazole rings are often undergo S-oxidation, N-oxidation, desulfurization, and oxidative cleavage, producing unstable low-level metabolites that require high resolution MS (HRMS) for accurate detection and structural identifications [4–6]. Because thiazole metabolism can generate electrophilic or reactive intermediates, early identification is essential to mitigate safety risks. *In silico* tools can predict probable soft spots, while *in vitro* systems such as liver microsomes, subcellular fractions, and hepatocytes help confirm metabolic pathways and identify structural elements requiring modification [4, 7, 11, 12].

Radiolabeled studies using preclinical species provide comparative metabolic profiles to ensure that they are exposed to human-relevant thiazole metabolites [13–23]. Modern LC-MS platforms, including triple quadrupole systems for quantitative analysis and hybrid ultra-high performance liquid chromatography (UHPLC) MS/MS instruments are widely used for structural elucidation due to their sensitivity and ability to detect diverse thiazole-derived metabolites [8, 9, 13]. Targeted (MRM) LC-MS metabolomics approaches further enhance metabolite coverage and confidence in identification [25–30].

Within this context, a new aminothiazole derivative, 19 monoaminothiazole (19MAT), was synthesized as part of a dengue virus (DENV)–focused discovery program. Subsequent research evaluated its pharmacokinetic profile, *in vitro* metabolic profile, oral bioavailability, and metabolite disposition [29]. A highly sensitive and selective LC–MS/MS method was developed and validated in accordance with ICH M10 and prevailing industry practices to facilitate comprehensive metabolite screening across the matrix [32, 33]. The primary objective was to know the absolute bioavailability of 19MAT following oral and intravenous administrations and to understand its metabolic disposition in rat plasma, urine, and feces, as well as in microsomal incubation systems.

In silico prediction (BioTransformer 3.0 and SMARTCyp 3.0) was used to predict the biotransformation and sites of metabolic liability and to understand the basis for subsequent experimental confirmation [34, 35]. A structural analogue of 19MAT was used as internal standard for

quantitative analysis. LC–MS/MS assay was rigorously assessed for accuracy, precision, recovery, matrix effects, and stability under diverse storage conditions, prior to its use [36]. This integrated experimental computational approach helped in identification of phase I and phase II metabolites, supported the understanding of metabolic pathways, and allowed a comprehensive assessment of PK characteristics. These data collectively furnish essential insights into the bioanalytical performance, pharmacokinetics, and biotransformation of 19MAT, hence endorsing its ongoing development as a potential antiviral candidate against DENV [29, 32–35].

MATERIALS AND METHODS

Chemical and reagents

Novel aminothiazole19MAT ($C_{18}H_{16}N_3O_2S$, 339.41, purity ≥97%) and its structural analogue 21MAT, which was used as an internal standard ($C_{18}H_{17}N_3O_3S$, 355.41, purity ≥97%), were synthesized as part of the research work obtained from BITS, Ranchi, Manesar. HPLC-grade solvents, acetonitrile, methanol, formic acid, ammonium formate, sodium phosphate, phosphate buffer sachet, Verapamil, nicotinamide adenine dinucleotide phosphate (NADPH)and dimethyl sulfoxide (DMSO), were procured from Sigma-Aldrich (Mumbai, India). Research grade (RandD) formulation excipients Propylene glycol (PG), N-methyl-2-pyrrolidone (NMP), and Solutol® HS 15 were procured from Sigma-Aldrich. Micro and semi-microbalances were sourced from Radwag (Mumbai, India) and used for weighing. Refrigerated centrifuge and micropipettes were from Eppendorf, Germany. Water dispensing system was from Evoqua, Xylem Inc., USA, used for all the reagents for the experiments.

LC-MS/MS analysis conditions

A triple quadrupole mass spectrometer SCIEX API4500™LC-MS/MS coupled with liquid chromatography (LC, from Shimadzu) and positive electrospray ionization (ESI) source were used for all the sample analysis. A reverse phase Waters Xterra RP® C_{18} (150 mm × 4.6 mm, 5 µm) column was used to separate the analyte and internal standard in the samples. The column oven was maintained at 40 °C, and the autosampler at 5 °C. Isocratic elution with aqueous phase of 5 mmol ammonium formate with formic acid (0.1% v/v) and organic phase of a combination of methanol and acetonitrile (95:5, v/v) with formic acid (0.1% v/v) were used in the chromatography. The overall ratio of aqueous to organic phase was 15:85%. A flow rate of 1 ml/min used for all the analysis with injection volume of 10 µl**. Electrospray ionization (ESI) source parameters were maintained as follows: collision gas (CAD) – 10, curtain gas (CUR) – 25, source gas1 (GS1) – 60, source gas2 (GS2) – 40, ion spray voltage-5500, temperature – 500 °C and dwell time of 200 milli seconds. In addition to these, compound-specific parameters were maintained as declustering potential (DP) of 100, entrance potential (EP) of 10, collision energy (CE) of 30, and collision cell exit potential (CXP) of 10, which were maintained common for both analyte and internal standard. The MRM transitions of 19MAT and internal standard were *m/z* 341.2→206.1, 341.2→136.1 (sum of the ions was used for the qualification), and *m/z* 357.2→152.3, respectively [31].

19MAT (Analyte) **21MAT (Internal standard)**

Fig. 1: Structures of 19MAT (Analyte) and 21MAT (Internal standard)

Calibration standard (CC) and quality control (QC) samples in rat plasma

Stock solutions of 19MAT were prepared in DMSO at 1 mg/ml. One stock was used as standard stock and diluted further to prepare calibration standards with 25.3, 50.5, 101, 202, 672, 1120, 3740, 8140, 17700, and 25300 ng/ml concentrations in DMSO. A separate stock was used to prepare quality control solutions with 24.7, 75.9, 253, 10100, and 20200 ng/ml concentrations. A stock solution of internal standard (21MAT, 1.0 mg/ml) was prepared in DMSO. A working solution of 1 µg/ml internal standard prepared in acetonitrile was used in the analysis.

To prepare calibration standards and quality control samples, 47.5 µl** aliquots of blank rat plasma were aliquoted, to which 2.5 µl** of calibration standard and quality control solutions were spiked and mixed. 150 µl** of internal standard working solution (1 µg/ml prepared in acetonitrile) was added to all the samples. The samples were vortex mixed for 10 min at 1500 rpm and centrifuged to separate the supernatant for 10 min at 14,000 rpm and at 4 °C. Organic supernatant of about 150 µl** was transferred into polypropylene shell vials and sealed. These samples were subjected to LC-MS/MS analysis. The final calibration curve range was 1.27 to 1270 ng/ml and QC concentrations of 3.80, 505, and 1010 ng/ml, respectively.

Method validation

Peak area ratios (peak area of analyte/internal standard) were used to measure the analyte concentration in the matrix. Linear regression analysis, $y = mx + C$, was adopted with a weighting factor ($1/x^2$), where C is the value of the y-axis intercept, m is the slope of the linear curve, x is concentration, and y is the peak area ratio [31].

System suitability

The instrument's suitability was assessed by evaluating the system precision by comparing the %RSD of the area ratios obtained after repeated injection of the extracted highest calibration standard sample. Precision of analyte and internal standard retention times were also assessed.

Specificity and selectivity

The objective was to assess the endogenous interference with the retention times of the analyte and internal standard in the analytical run. The method's specificity was assessed using blank plasma from six different lots, blank plasma spiked with analyte and internal standard, and pharmacokinetic study samples. Similarly, selectivity was assessed at 1.27 ng/ml concentration, which was considered as the lower limit of quantification (LLOQ). Six lots of interference free blank plasma was spiked at LLOQ level, and the signal-to-noise ratio was calculated against the mean baseline noise near the analyte retention time [36].

Linearity (Calibration curve)

Calibration curve was constructed using 10 non-zero standards (1.27, 2.53, 5.05, 10.1, 33.6, 56.0, 187, 407, 885, and 1270 ng/ml) covering the validated concentration range of 1.27 ng/ml to 1270 ng/ml. Linearity was assessed by least-squares linear regression with a weighting factor ($1/x^2$). The calibration model was accepted if the coefficient of determination (r^2) was ≥0.99. The standard curve was plotted using the peak area ratio of 19MAT (y) to the internal standard to the concentration(x) to assess the linearity [31].

Precision and accuracy

Three batches each of CC (10 standards) and six sets of QCs were used to validate intra-and inter-day precision and accuracy. For the evaluation of accuracy and precision, QC samples of 4 non-zero concentrations (1.24, 3.80, 505, and 1010 ng/ml) were processed on the same day (intra-day) and three consecutive days (inter-day). The acceptance criteria followed for accuracy of each back-calculated standard concentration was within ±15% of the nominal value, except for LLOQ, which was permitted a deviation of ±20%. At least 75% of all calibration standards, including the LLOQ and upper limit of quantification (ULOQ), were required to meet these criteria [31-33].

Matrix recovery

Plasma recovery of 19MAT was determined at 3 QC levels: LQC (low-level QC), MQC (mid-level QC), and HQC (high-level QC) in six replicates. The area ratios of analyte to internal standard from extracted QC samples were compared against the aqueous spiked samples without matrix. The recovery of the internal standard in the matrix was also assessed, similarly at 1000 ng/ml concentration.

Matrix effect/factor

The influence of rat plasma on the recovery of analyte (at LQC and HQC levels) and internal standard was assessed as a matrix effect. The peak areas of post-extracted sample were compared to the comparator sample, which was free from matrix.

Matrix stability

Stability of 19MAT was assessed at QC concentrations (3.80, 505, and 1010 ng/ml) in rat plasma. The concentrations were tested for stability under following conditions: (1) bench top for 5 h, (2) at autosampler for 24 h; (3) over five freeze–thaw cycles at-20 °C and-70 °C and (4) long term stability of 45 d of storage at-20 °C and-70 °C [31-33].

***In silico* metabolism prediction**

BioTransformer 3.0 (software version 3.0), *in silico* module which predicts small-molecule metabolism in mammals and helps scientists identify metabolites based on the metabolism prediction was used for initial survey on the prediction of metabolites of 19MAT before actual comparison with experimental samples. BioTransformer 3.0 uses knowledge-based and machine learning based approaches to predict small-molecule metabolism. SMILE file of 19MAT was used along with EC-based, CYP450, Phase II, human gut microbial and environmental microbial modules [34].

SMARTCyp3.0 prediction of metabolism sites

The prediction on the sites for metabolism from cytochrome P450-mediated drug metabolism was referred from SMARTCyp 3.0 server web application (www.farma.ku.dk/smartcyp, accessed on 02 February 2025). SMARTCyp3.0 used for P450 site-of-metabolism prediction was applied using SMILES inputs, with scoring based on activation energy, accessibility, and predicted 2D solvent-accessible surface area [36-38].

Intrinsic clearance of 19MAT in rat liver microsomes

The *in vitro* metabolism of 19MAT was investigated in rat liver microsomes, along with half-life and intrinsic clearance (CL_{int}). Liver microsomes procured from XenoTech LLC (Kansas, USA) were used at protein concentration of 20 mg/ml. The experiment was conducted at 0.5 µM for test compound and Verapamil was used as positive control [40].

Sodium phosphate buffer, liver microsomes and NADPH were incubated for 10 min at 37 °C. Addition of 2.5 µl** of 100 µM test compound has initiated the reaction. Aliquots of samples were collected at 0, 5, 10, 20, and 30 min, and mixed with acetonitrile to stop the reaction. NADPH-free control reactions were performed with similar conditions and samples were collected at 0 and 30 min. The samples were mixed with internal standard, centrifuged at 4,000 rpm for 20 min and supernatant was used for LC-MS/MS analysis.

The time-dependent metabolism of 19MAT was monitored using LC-MS/MS method. The data was fitted to the one phase exponential decay equation ($A = Aoe^{-kt}$) using GraphPad Prism® software (by Dotmatics). The half-life ($t_{1/2}$) generated by the software has been reported. Intrinsic clearance was calculated using the formula.

$$CL_{int} = \frac{k \times \text{volume of reaction mixture (µL)}}{\text{protein content (mg)}}$$

where, k = decay rate constant (min-1)

***In vitro* metabolite identification in rat liver microsomes**

Rat liver microsomes suspended in a NADPH-generating system at 0.5 mg/ml with a 0.1 M phosphate buffer (pH 7.4) were used in the experiment. Experiment was conducted at final incubation concentration of 0.5 µM of 19MAT to initiate the reactions after a preincubation for 5 min at 37 °C. 19MAT free reaction mixture (Sodium phosphate buffer, liver microsomes and NADPH) was used as control. Samples were collected at 0, 30, 60 and 120 min and mixed with acetonitrile. In all cases, NADPH-free control reactions were performed in a similar manner, and samples were collected at 0 and 120 min and quenched in acetonitrile. The samples quenched were centrifuged at 14,000 rpm for 10 min and an aliquot of supernatant was taken for LC-MS/MS analysis identification of metabolites.

Pharmacokinetic study

Six male Sprague–Dawley rats (weight 200±20 g) used were obtained from Vivo Biotech (Hyderabad, India). Formulations prepared with 10 % NMP, 30 % PG, 30 % Solutol HS 15, and q. s sterile water for injection were used in the study. The selection of vehicle composition was for ensuring adequate solubility, dose accuracy, and physiological compatibility for both intravenous and oral administration. For the oral formulation, the vehicle choice was to enhance drug solubilization, stability in the gastrointestinal environment and intestinal conditions. For the intravenous formulation, pH adjustment was within a physiologically acceptable range (pH 6.5–7.5) to reduce the risk of vascular irritation and maintain chemical stability. Osmolarity was controlled to be close to isotonic conditions (~280–320 mOsm/kg) to avoid hemolysis or vein irritation. These parameters were optimized to ensure smooth IV administration and minimize formulation-related variability in pharmacokinetic outcomes. The

rats were divided into two groups of three each. Overnight fasted rats of the first group were dosed intravenously at a 1 mg/kg dose with a 2 ml/kg dose volume through the tail vein. The second group of rats were treated orally at 10 mg/kg dose with a 10 ml/kg dose volume. These doses are selected with an objective of complete absorption, first-pass metabolism, and quantifiable plasma levels, while the IV dose is kept lower to avoid excessive systemic exposure. The 10-fold difference therefore reflects a pharmacokinetic rationale aimed at compensating for low or variable oral bioavailability, enabling reliable estimation of PK parameters. Formulations of these dosages were at 0.5 mg/ml and 1 mg/ml of 19MAT, respectively. Pharmacokinetic study was conducted in compliance with institutional animal ethics guidelines and approved by the institutional animal ethics committee (IAEC Approval No.: Proposal No. ADG-42_PKR/May-2022, dated 27 May 2022) [17, 19, 23].

Sample collection

Plasma samples were collected from the rats after IV treatment at pre-determined timepoints of 0 (pre-dose), 0.083, 0.25, 0.5, 1, 2, 4, 8, and 24 h post-dose. Similarly, samples were collected at 0 (pre-dose), 0.25, 0.5, 1, 2, 4, 8, and 24h post-dose from rats treated orally. At each time point, about 0.2 ml of blood was collected from the retro-orbital plexus into the polyethylene tubes containing dipotassium ethylenediaminetetraacetic acid (K_2EDTA) at 20 µl** per ml of blood (200 mmol K_2EDTA in water). For plasma separation, all the blood samples were centrifuged at 14000 rpm at 4 °C for 10 min. The separated plasma samples were stored in labeled containers at-70±10 °C until analysis. In addition, the urine and fecal samples were collected separately from 0 to 6 h and 6 to 24 h after dosing.

Sample preparation for metabolite identification

Plasma

Sample aliquots of 50 µl** were mixed with 150 µl** of internal standard (1000 ng/ml in acetonitrile), which precipitated the proteins and extracted the analytes of interest [31]. All the samples were vortexed for 10 min at 1500 rpm and centrifuged for 10 min at 14,000 rpm (~11000 g, 4 °C). After separation, 150 µl** of the organic supernatants were transferred into polypropylene shell vials and sealed with polyethylene plugs. The samples were injected into the LC-MS/MS apparatus in aliquots of 10 µl** each for analysis.

Urine

To the aliquots of urine samples, 2 volumes of acetonitrile-water (50:50, v/v) were added and vortexed for 20 min at 1500 rpm. The samples were centrifuged for 15 min at 14,000 rpm (~11000 g, 4 °C). The supernatant was dried under a nitrogen stream, and dried pellets were reconstituted with100 µl** of acetonitrile–water (50:50, v/v) and used for metabolic profiling and identification [15].

Feces

Each fecal sample was thoroughly mixed with water (three times the weight) and homogenized to get a uniform slurry. To aliquots of fecal homogenates, three times the volume of acetonitrile-water (50:50, v/v) was added for the proper extraction of the analyte and vortexed for 20 min at 1500 rpm. Samples were centrifuged at 14,000 rpm (~11000 g, 4 °C) for 15 min to separate the organic supernatant. The supernatant was dried under a nitrogen stream and reconstituted with 100 µl** of acetonitrile–water (50:50, v/v) and used for metabolic profiling and identification [15].

RESULTS

Method development

The chromatographic conditions were optimized for sufficient sensitivity for detecting 19MAT and its internal standard. The method development trials showed that both analytes eluted within a narrow polarity range and did not require a gradient separation from endogenous matrix components. Isocratic elution was selected over gradient due to the chromatographic behavior of 19MAT and internal standard with sufficient retention, resolution, and peak symmetry under a fixed mobile-phase composition. After evaluating combination of various aqueous and organic solvents (both isocratic and gradient elution) for setting up the chromatography, an isocratic combination of 5 mmol ammonium formate with formic acid (0.1% v/v) and mixture of methanol and acetonitrile (95:5, v/v) with formic acid (0.1% v/v) were found suitable in the ration of 15:85, v/v. These conditions were used in all the LC-MS/MS analysis. Also, a good separation was achieved by using Xterra RP® C18 (150 mm X 4.6 mm, 5 µm) column for analyte and internal standards after evaluating many columns of different brands and stationary phases. Positive ionization (ESI+) mode was able to provide proper signal for both 19MAT and its internal standard, and stable MRM transitions were used in the quantification.

LC-MS/MS method validation

System suitability

To confirm the system's suitability through the experiments, on each occasion the % coefficient of variation (%CV) for the peak area ratio (analyte to internal standard) of six injections at the ULOQ level was assessed. The retention times of both analyte and internal standards were consistently within±0.5 min during method validation, and % CV was ≤ 2% for both peak area ratio and retention times.

Specificity and selectivity

All six lots of blank plasma samples did not show any interference at the retention time of 19MAT and internal standard, confirming the specificity of the analytical method. The selectivity of the method was assessed based on which 1.27 ng/ml was selected as the LLOQ concentration. The method demonstrated acceptable accuracy and precision at the LLOQ which was within ±20% of the nominal concentration, and within-run precision (%RSD) was ≤20%, confirming the reliability of quantification at the lowest level. These results confirm that the assay is sensitive enough to detect and quantify the analyte at low plasma concentrations.

Linearity

The calibration curves drawn on different days of experiments were found to be linear using the least squares regression of the $1/x^2$ weighting factor. The coefficient of determination (R^2) value was more than 0.99 for all runs, indicating an adequate linear fit. Analyst® 1.7 was used for data collection, integration, and quantification. On each occasion, the percentage deviations of the back-calculated concentrations for calibration standards were within±15% of the nominal. At LLOQ, the accuracy was within±20% of the nominal value. The results confirmed that the LC-MS/MS method had a proper instrument signal and consistent response, which was reproducible across all the experiments.

Precision and accuracy

Both percentage relative errors and % relative standard deviations were used to determine accuracy and precision. The intra-day accuracy was in the range of 89.70 to 107.49%, and the inter-day accuracy was within the range of 85.00 to 105.57%. The intra-day and inter-day precision values

were less than 10%. Acceptance criteria of±15% from nominal concentrations was followed for calibration standards except for LLOQ for which a limit of± 20% was maintained. The results were within the acceptance limits as the ICH M10 guidelines. The inter-day precision near the LLOQ showed variability of approximately 10% (≤20% at the LLOQ). While this level of variability is considered acceptable for low-concentration measurements which might be signal variation, leading to slightly increased day-to-day fluctuations. Despite this, the observed precision remains well within allowable limits and does not compromise the reliability of LLOQ-level quantification. The data is presented in table 1.

Matrix recovery

The recovery of 19MAT and internal standard from rat plasma was ranging from 48 to 63% and 48 to 51%, respectively, evaluated at LQC, MQC, and HQC levels. Although the recovery was moderate (due to protein binding of the analyte limiting the extraction from matrix, extraction efficiency of the method, and physicochemical properties of the analyte (e. g., polarity, solubility), it was consistent and reproducible, meeting the acceptance criteria for accuracy and precision during method validation. The data can be referred to from table 2.

Matrix factor

The % CV was less than ±15%, and the matrix factor was within the allowed range of 1.06±0.00 at the LQC level and 1.20±0.03 at the HQC level. Apparent inconsistency in the matrix factor calculated from post-extraction spiked samples, with RSD values of 14.37% and 0.00% reported at different QC levels likely from very low absolute signal variation between replicates or instrument-precision limits. Such differences are not uncommon and may be influenced by sample composition, endogenous substances, or slight extraction-recovery variations across lots. Matrix factor greater than 1 indicates possible ionization enhancement, which are expected part of LC–MS/MS analysis and is acceptable as long as the effect is consistent, reproducible, and does not compromise accuracy or precision of the method which was confirmed as both accuracy and precision met validation criteria, confirming that the matrix effect did not adversely impact quantification. The data are presented in table 2.

Matrix stability

19MAT was stable in rat plasma for five hours when stored at room temperature. Similarly, the analyte was also stable in the matrix for up to five freeze-thaw cycles at-20 °C and – 70 °C. Also, 19MAT was stable in rat plasma up to 45 d at both – 20 °C and – 70 °C. All the stability evaluations were made at LQC and HQC levels, and at all the above experimental conditions, with % changes less than 10 at all conditions. The experimental findings can be referred to in table 3. In addition, the stability of 19MAT and the internal standard in the stock solution was evaluated for 7 d (short-term) at room temperature and for approximately 3 mo (long-term) at 4 °C.

Table 1: Precision and accuracy summary of the method

Analyte	Concentration(ng/ml)	QC level	%RSD		RE (%)	
			Inter day	Intra Day	Inter day	Intra Day
19MAT	1.22	LLOQQC	10.79	6.26	-1.61	0.81
	3.75	LQC	9.94	6.56	1.79	3.68
	500	MQC	10.36	3.91	1.89	4.75
	1000	HQC	5.27	4.09	6.04	6.63

Inter-day (n = 18) and intra-day (n = 6); RE: Relative error, %RSD: Relative standard deviation; LLOQQC: Lower Limit of Quantification Quality Control, LQC: Low Quality Control; MQC: Mid Quality Control; HQC: High Quality Control; QC: Quality Control

Table 2: Recovery and matrix factor

Analyte	QC level	Concentration(ng/ml)	Recovery mean (%)	Matrix factor	RSD (%)
	LQC	3.75	54.10	1.06	0.00
19MAT	MQC	500	63.52		
	HQC	1000	47.78	1.20	2.50

LQC: Low Quality Control; MQC: Mid Quality Control; HQC: High Quality Control, Recovery presented in mean %; QC: Quality Control

Table 3: Stability in rat plasma samples under different storage conditions

Storage condition	QC level	Concentration (ng/ml)		RE (%)
		Nominal	Measured	
Short term	LQC	3.80	3.57	-6.05
(Room temperature, 5h)	HQC	1010	1018	0.79
Autosampler	LQC	3.80	3.52	-7.36
(5 °C, 24h)	HQC	1010	1019	0.89
Freeze thaw	LQC	3.80	3.81	0.26
(5 Cycles,-20 °C)	HQC	1010	874	-13.46
Freeze thaw	LQC	3.80	3.45	-9.21
(5 Cycles,-70 °C)	HQC	1010	889	-11.98
Long term	LQC	3.80	3.47	-8.68
(-20 °C, 45 d)	HQC	1010	885	-12.38
Long term	LQC	3.80	3.80	0.00
(-70 °C, 45 d)	HQC	1010	1027	1.68

Measured concentration presented as mean (n=6); LQC: Low Quality Control; HQC: High Quality Control; h-hour; QC: Quality Control

***In silico* metabolite prediction**

BioTransformer 3.0 has predicted about 6 phase I (first level reactions) and a single primary phase II metabolite. *In silico* predictions provided information related to the type of metabolic reactions, enzymes responsible for metabolism, isotope mass of metabolites, chemical formula, and the protected structure of the metabolites. This information was used in the metabolite prediction as a first step, and the data was compared with the obtained from LC-MS/MS analysis of *in vitro* and PK samples. The metabolite predictions from BioTransformer 3.0 are presented in table 4.

Site of metabolism (SOM) prediction using SMARTCyp 3.0

Fig. 2 shows the results of the 19MAT molecule sites liable for metabolism byCYP450. The SMARTCyp 3.0 standard algorithm (CYP3A4) demonstrated that the potential sites of modifications were C.15 site (Score = 51.5; Energy = 62.2), C.1 site (Score = 58.4; Energy = 66.4), and C.8 site (Score = 63.3; Energy = 69.4). The SMARTCyp 3.0 CYP2D6 algorithm indicated that the potential 19MAT sites of modifications were C.15 site (Score = 59.5; Energy = 62.2), C.20 site (Score = 89.4; Energy = 77.2), and C.1 site (Score = 91.1; Energy= 66.4). The SMARTCyp3.0 algorithm has also highlighted the potentialCYP2C9 related modifications at C.15 site (Score = 59.5; Energy = 62.2), C.20 site (Score = 87.8; Energy = 77.2), and C.1 site (Score = 88.0; Energy = 66.4). The lowest score with theCYP3A4 algorithm wasN.6 (Score = 87.0; Energy = 92.1). With applying the SMARTCyp3.0 CYP2D6 algorithm, the most discouraged fragmentationwasN.6 (Score = 118.4; Energy = 92.1) and based on the SMARTCyp 3.0 CYP2C9 algorithm, the least recommended fragmentationwasN.6 (Score = 115.2; Energy= 92.1). Based on the three different SMARTCyp3.0 algorithms, the primary SOM in 19MAT was C.15 which is a methoxy group [37-39].

Table 4: *In silico* metabolite prediction data from BioTransformer 3.0

Reaction type	Major isotope mass (Da)	Chemical formula	Reaction info	Predicted structure
Phase I metabolism				
O-Dealkylation	325.0884	$C_{17}H_{15}N_3O_2S$	Enzyme: Cytochrome P450 1A2	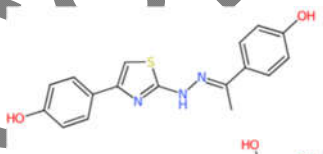
2-Hydroxylation of 1,4-disubstituted benzene	355.099	$C_{18}H_{17}N_3O_3S$	Enzyme: Cytochrome P450 1A2	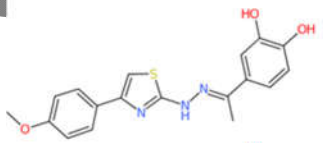
2-Hydroxylation of 1,4-disubstituted benzene	341.0834	C17H15N3O3S	Enzyme: Cytochrome P450 1A2	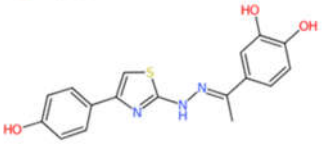
2-Hydroxylation of 1,4-disubstituted benzene	371.0939	C18H17N3O4S	Enzyme: Cytochrome P450 1A2	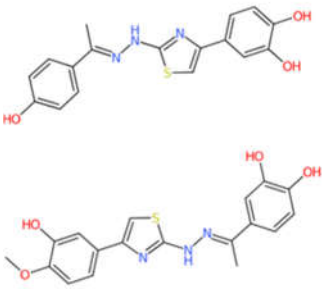
S-Oxidation of sulfoxide to sulfone	387.0888	C18H17N3O5S	Enzyme: Cytochrome P450 2C9	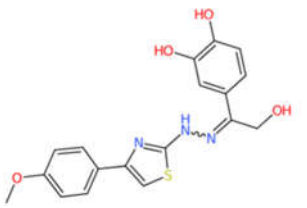
SNP-Oxidation	355.09906	C18H17N3O3S	Enzyme: Cytochrome P450 2E1	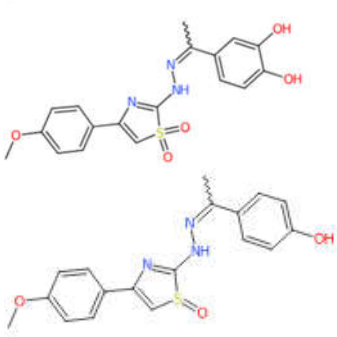
Phase II Metabolism				

Aromatic OH-glucuronidation	515.1362	C24H25N3O8S	Enzyme: UDP-glucuronosyltransferase	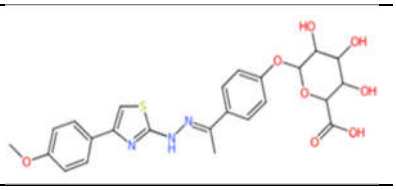

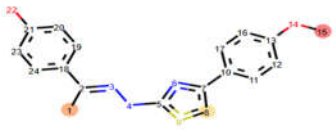

3A4 Ranking	Atom	3A4 Score	Energy	2DSASA	Span2end	Relative Span	Similarity
1	C.15	51.5	62.2	66.4	0	1.0	1.0
2	C.1	58.4	66.4	50.8	4	0.8	0.7
3	C.8	63.3	69.4	27.0	6	0.6	0.3
4	S.9	63.6	70.0	46.8	7	0.6	0.7
5	N.4	66.9	72.0	14.0	7	0.6	0.3
6	C.20	69.0	77.2	30.5	2	0.9	0.7
7	C.12	69.6	77.2	28.6	3	0.8	0.7
8	C.19	73.2	80.8	26.7	3	0.8	0.7
9	C.11	73.8	80.8	26.1	4	0.8	0.7
10	N.6	87.0	92.1	15.4	7	0.6	0.3

(a)

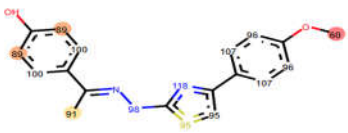

2D6 Ranking	Atom	2D6 Score	Energy	2DSASA	Span2end	N+dist	Similarity
1	C.15	59.5	62.2	66.4	0	0	1.0
2	C.20	89.4	77.2	30.5	2	0	0.7
3	C.1	91.2	66.4	50.8	4	0	0.7
4	S.9	95.0	70.0	46.8	7	0	0.7
5	C.8	95.2	69.4	27.0	6	0	0.3
6	C.12	96.2	77.2	28.6	3	0	0.7
7	N.4	98.3	72.0	14.0	7	0	0.3
8	C.19	99.8	80.8	26.7	3	0	0.7
9	C.11	106.6	80.8	26.1	4	0	0.7
10	N.6	118.4	92.1	15.4	7	0	0.3

(b)

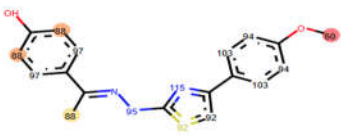

2C9 Ranking	Atom	2C9 Score	Energy	2DSASA	Span2end	COO-Dist	Similarity
1	C.15	59.5	62.2	66.4	0	0	1.0
2	C.20	87.8	77.2	30.5	2	0	0.7
3	C.1	88.0	66.4	50.8	4	0	0.7
4	S.9	91.8	70.0	46.8	7	0	0.7
5	C.8	92.0	69.4	27.0	6	0	0.3
6	C.12	93.8	77.2	28.6	3	0	0.7
7	N.4	95.1	72.0	14.0	7	0	0.3
8	C.19	97.4	80.8	26.7	3	0	0.7
9	C.11	103.4	80.8	26.1	4	0	0.7
10	N.6	115.2	92.1	15.4	7	0	0.3

(c)

Fig. 2: Site of metabolism prediction for 19MAT using SMARTCyp3.0 for (a) CYP3A4, (b) CYP2D6, and (c) CYP2C9

In vitro intrinsic clearance of 19MAT in liver microsomes

The intrinsic clearance and half-life values in rat, and human liver microsomes are presented in the table below.

Table 5: Results of *in vitro* intrinsic clearance in rat and human liver microsomes

Test item	Liver microsomes	0.5 mg/ml protein concentration			
		Half-life (min)		CL_{int} (µl/min/mg protein)	
		SET-1	SET-2	SET-1	SET-2

19MAT	Rat	4.95	5.04	34.56	35.06
	Human	30.3	31.1	5.57	5.66
Verapamil	Rat	15.57	15.97	81	77
	Human	11.24	10.89	113	121

Final incubation concentration was 0.5 µM; CL_{int}: Intrinsic clearance; Low Clearance Category:<8.6 µl**/min/mg protein (Human); High Clearance Category:>47 µl**/min/mg protein (Human)

A clearance value of<8.6 µl**/min/mg protein will be considered as low clearance and>47 µl**/min/mg protein as high clearance in human liver microsomes [40]. The values in rat liver microsomes are<15.8 µl**/min/mg protein for low and>86.1 µl**/min/mg protein for high clearance values, respectively.

The data showed that 19MAT undergone high metabolism and medium clearance in rat liver microsomes with a half-life of<6 min and slow metabolism and low clearance in human liver microsomes with a half-life of>30 min.

***In vitro* metabolite identification of 19MAT in rat liver microsomes**

Mass spectroscopic analysis of 19MAT

The parent 19MAT was analyzed using LC-MS/MS. The $[M+H]^+$was detected at the *m/z* 340.4, at the retention time of 38.90 min. In the product ion scan mode (MS_2), three major fragment ions at *m/z*136.3and 206.1 were detected. The fragments of *m/z*136.3 and 205.1 might be a possible breakage of hydrazinyl bond between N-N between 6 and 7 positions. However, the fragment at m/z 164.3 could be a possible opening of thiazole ring opening at positions 2 and 3.

Mass spectroscopic analysis of microsomal incubation samples

For identifying the metabolites, the samples were compared against the blank sample without 19MAT. There were ions with *m/z* 326.4 (possible O-dealkylation), 338.4 (dehydrogenation) and 372.4 (dihydroxylation) observed in Q1 scan. However, due to less abundance these were not found significant, and no further fragmentation confirmation could be conducted.

M1 was detected at the retention time of about 33.0. The molecular ion $[M+H]^+$at *m/z* 356.9 with a mass difference of 16, suggesting a possible hydroxylation. The fragmentation pattern shown ions at *m/z* 205.2, 164.0 and 152.3 suggesting possible modification around substituted phenolic ring and in line with the fragmentation pattern with that of parent. The fragmentation pattern of M1 has been presented in fig. 3.

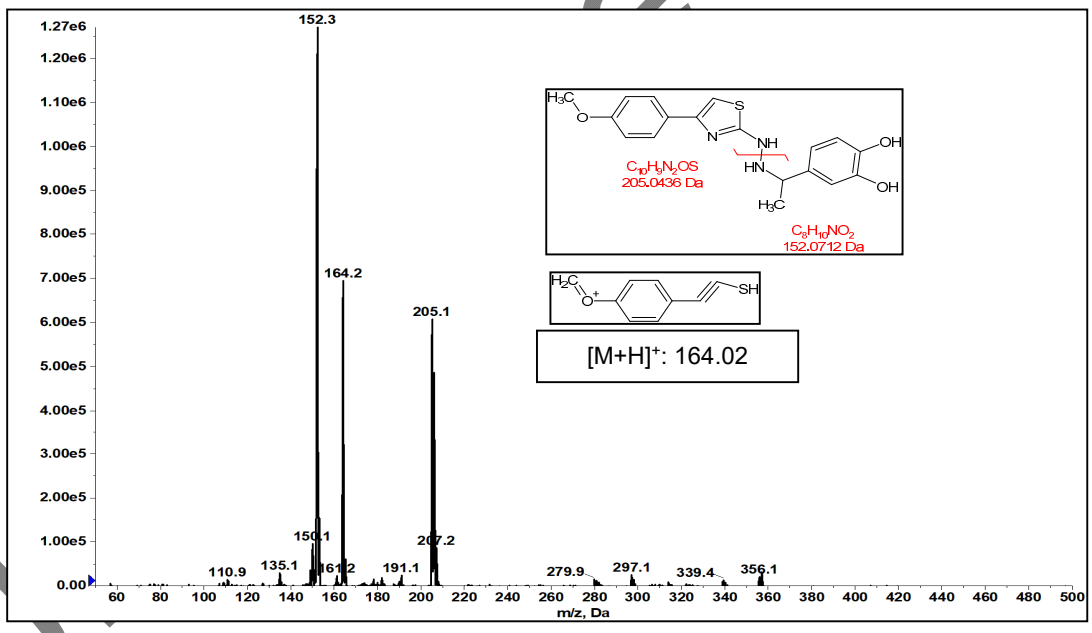

Fig. 3: Fragmentation pattern of M1 metabolite

Pharmacokinetic analysis

Noncompartmental analysis (linear trapezoidal method; Phoenix™ v8.0) was used to determine the pharmacokinetics of 19MAT following oral gavage and intravenous administration. After oral administration, 19MAT exhibited rapid absorption which was confirmed by its shorter time to reach maximum plasma concentration (T_{max}) with measurable systemic exposure and a longer mean residence time (MRT) when compared with intravenous dosing showing a prolonged absorption phase. Absolute oral bioavailability was 23.82%, while the intravenous data indicated extensive distribution [19]. The data is tabulated in table 6. The concentration time curves can be referred to from Figure 4 (a) and (b).

Table 6: Pharmacokinetic parameters after IV and PO administration to rats

Parameters	Units	PO (10 mg/kg)	IV (1 mg/kg)

AUC_{0-t}	h*(ng/ml)	363±44	865±256
AUC_{inf}	h*(ng/ml)	376±24.4	865±256
MRT_t	h	7.82±0.518	2.19±0.173
T_{max}	h	0.417±0.144	0.139±0.0964
$t_{1/2}$	h	4.20±3.14	1.21±0.49
C_{max}	ng/ml	72.7±15.3	958±371
CL	mL/h/kg	-	1218±345
V_d	mL/kg	-	1977±525
F (%)	-	23.82	-

AUC0–t (AUC0–inf), area under the analyte concentration versus time curve from time 0 to t h (inf); MRT0–t, mean residence time at time 0–t (inf); T_{max}, the time of maximum concentration; $t_{1/2}$, terminal half-life; C_{max}, maximum concentration; CL, clearance; V_d, apparent volume of distribution; F (%), absolute bioavailability; PO, per oral; IV, intravenous [15]; Data presented as mean±SD (n=3)

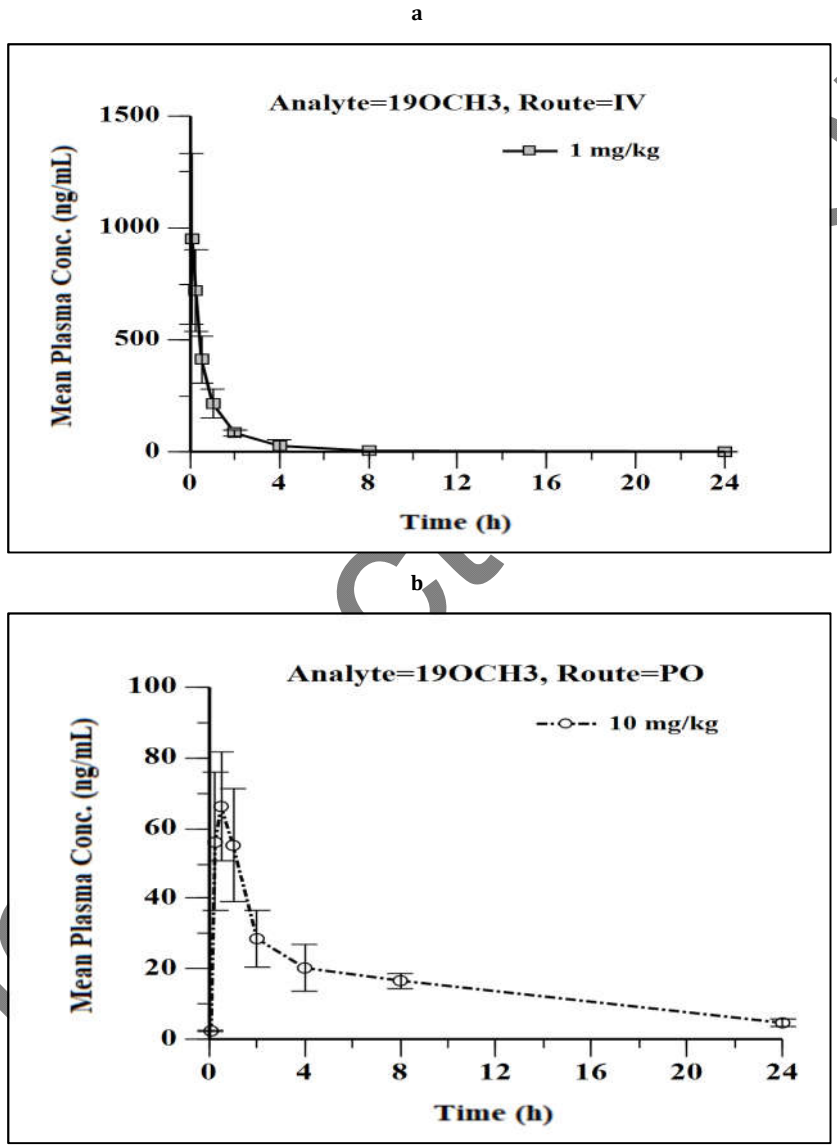

Fig. 4: Mean (±SD) plasma concentration–time profile of 19MAT in rats following (a) intravenous (1 mg/kg) and (b) oral (10 mg/kg) administration (n=3)

Identification of metabolites from rat samples

Product ion scanning (MS2)

Ionization of 19MAT showed a molecular ion peak at *m/z* 341.1. This observed value (341.1) is very close and within normal instrumental tolerance, especially for low-resolution or unit-resolution MS. In the triple quadrupole analyzer, the parent ion was fragmented into two primary daughter ions (with abundance), *m/z* 136.1 and *m/z* 206.1.

The information related to all metabolites was listed in table 7, including retention time (t_R), theoretical and observed molecular mass, major fragment ions, and possible structural modifications. The possible structure and its fragments are presented in fig. 5(a).

M1 metabolite (m/z 356)

M1 metabolite was detected at a retention time (t_R) of about 16.88 min in the full scan mode. This metabolite was detected in all three matrices (plasma, urine, and feces). Based on the molecular ion, the metabolite formed because of hydroxylation or N/S oxidation, in addition to the 19MAT structure. The possible structure and its fragments are presented in fig. 5 (b). The addition of hydroxy group attachments was predicted to be on each side of the phenyl rings. The fragmentation pattern of the metabolite was similar to that of the parent, with one fragment having *an m/z* of 164, and the second one was *m/z* 152**,** which might have undergone hydroxylation modification. The third common fragment was at *m/z* 205.

M2 metabolite (m/z 372)

In the full scan mode, M2 metabolite was detected at a retention time (t_R) of about 16.55 min. This metabolite could be a di-hydroxylation of the parent 19MAT and was detected in all three matrices (plasma, urine, and feces) with good abundance. The predicted chemical formula is $C_{18}H_{17}N_3O_4S$.

M3 metabolite (m/z 326)

At about 16.45 min in chromatography, an M3 metabolite with a chemical formula of $C_{17}H_{15}N_3O_2S$ was detected, which is a possible O-dealkylation. This metabolite was not common and was detected only in feces samples. The possible structure and its fragments are presented in fig. 5(*c*). The fragmentation pattern of the metabolite is similar to that of the parent, with fragments *m/z* 136 and *m/z* 191**,** which might have lost the alkyl group.

M4 metabolite (m/z 516)

M4 metabolite was one of the abundant metabolites eluted at about 15.99 min in the chromatography. The chemical formula is $C_{24}H_{25}N_3O_8S$, possibly due to the possible aromatic OH-glucuronidation catalyzed by UDP-glucanosyltransferase. This metabolite was detected in all three matrices (plasma, urine, and feces). The possible structure and its fragments are presented in fig. 5 (d). The fragmentation pattern of the metabolite confirms the modification to the parent ion of *m/z* 340 with fragments of *m/z* 205and *m/z* 136. A neutral loss of m/z 176 further confirmed the formulation of the glucuronide metabolite.

M5 metabolite (m/z 388)

The M5 metabolite was abundant and eluted at about 15.51 min in the chromatography. Its chemical formula is$C_{18}H_{17}N_3O_5S$, which was possible hydroxylation followed by oxidation at S. This metabolite was detected only in plasma and urine, and it was detected in less abundance.

M6 metabolite (m/z 342)

M6 metabolite is one of the less abundant metabolites eluted at about 15.00 min in the chromatography. Its chemical formula, $C_{17}H_{15}N_3O_3S$, suggests a possible dealkylation followed by hydroxylation. This metabolite was detected in all three matrices (plasma, urine, and feces).

M7 metabolite (m/z 502)

A possible dealkylation followed by aromatic OH-glucuronidation catalyzed by UDP-glucanosyltransferase resulted in M7 metabolite, one of the highly abundant metabolites eluted at about 11.52 min in the chromatography. This metabolite was detected in only feces. The metabolite was less sensitive and less abundant in plasma and urine. The formulation of the glucuronide metabolite was further confirmed by a neutral ion of *m/z* 176.

Fig. 5 represents the fragmentation pattern of parent 19MAT (a), hydroxylation metabolite (b), O-dealkylation (c) and glucoronide metabolites (d), obtained from the samples of pharmacokinetic study and LC-MS/MS analysis.

Table 7 presents a summary of the identified and predicted metabolites with masses and fragments. The predicted metabolic pathway of 19MAT is presented in fig. 6.

a

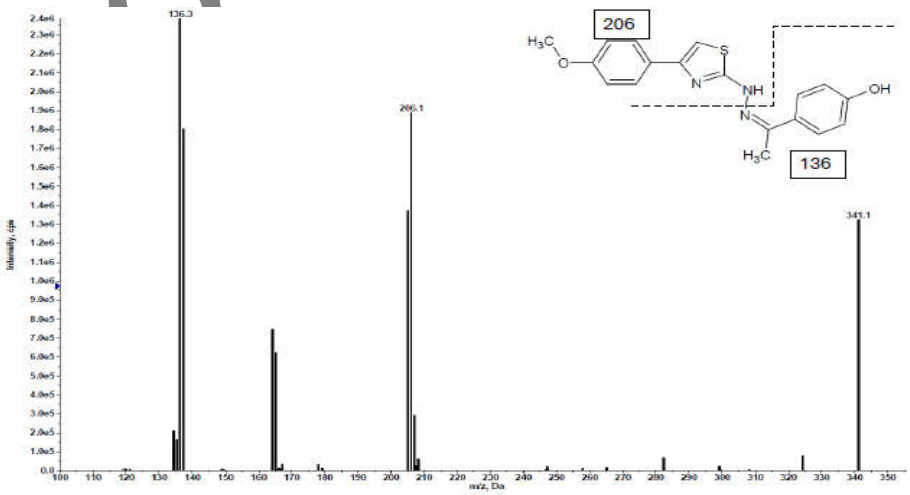

b

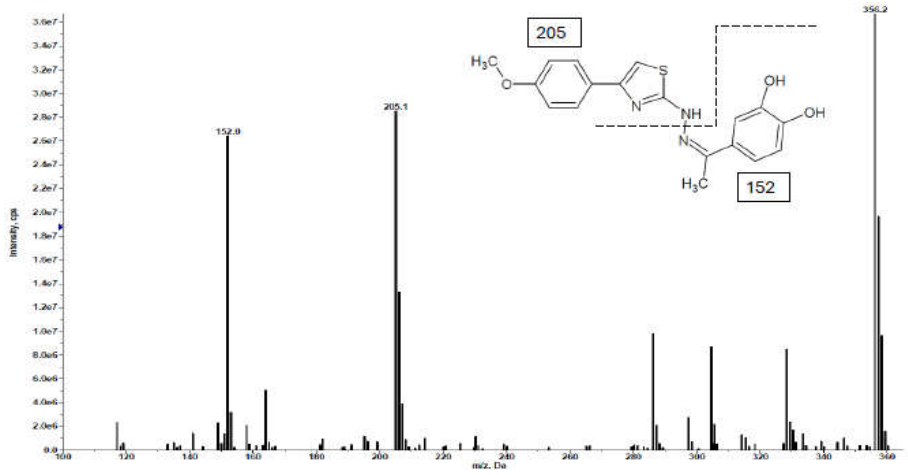

c

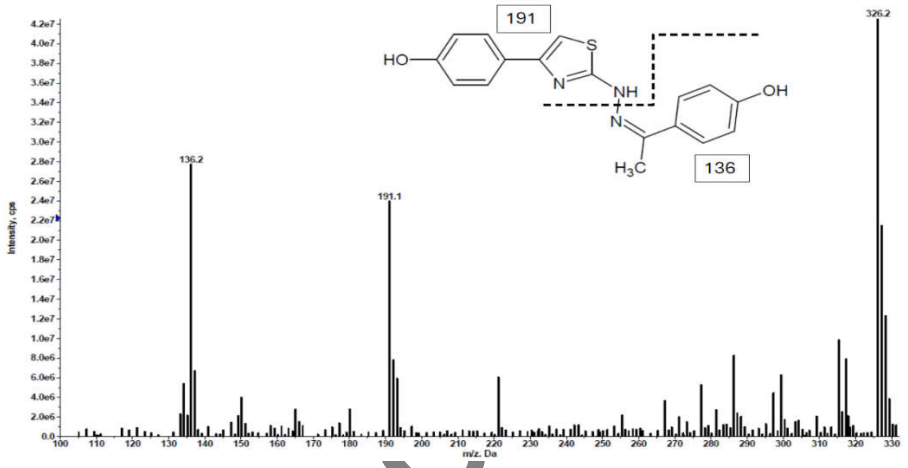

d

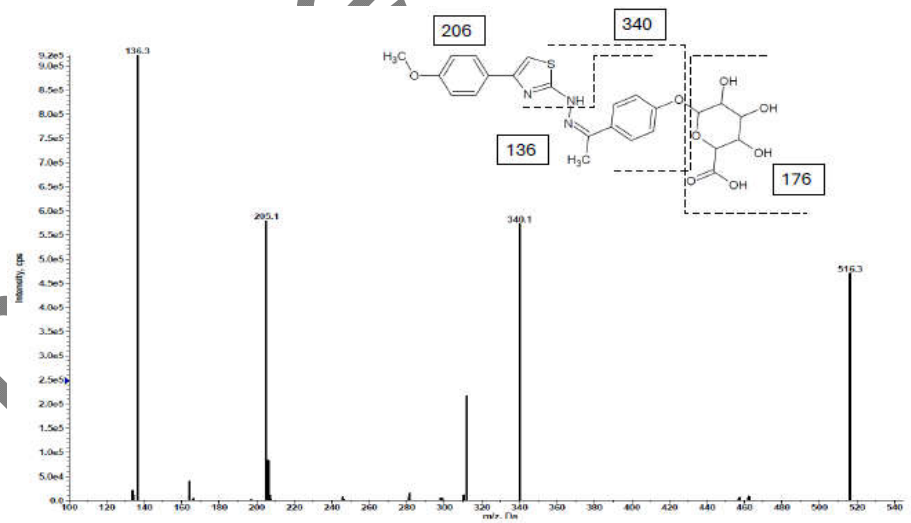

Fig. 5: (a). Fragmentation pattern of parent (*m/z: 341*), (b). Fragmentation pattern of hydroxylation metabolite (*m/z: 356),* (c). Fragmentation pattern of O-dealkylation metabolite (*m/z: 326)* and (d). Fragmentation pattern of glucuronide metabolite (*m/z: 516)*

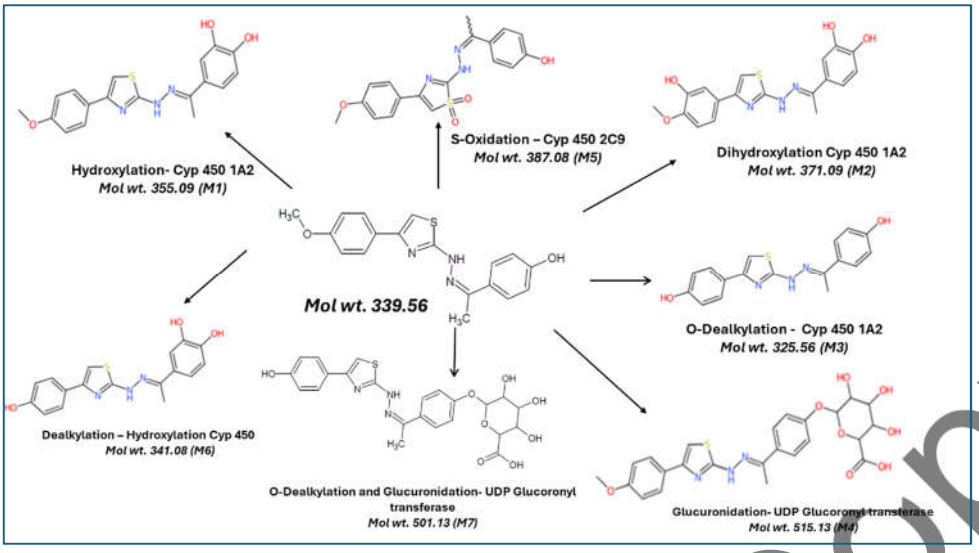

Fig. 6: Proposed major metabolic pathways of 19MAT in rats based on *in vivo* metabolite identification in plasma, urine, and feces. Metabolites M1–M7 correspond to those listed in table 7

Table 7: Metabolites of 19MAT identified in rat samples

Metabolite code	Retention time (min)	Theoretical mass (m/z)	Observed mass (m/z)	Product ion (m/z)	Detected matrix	Proposed biotransformation
Parent	18.46	340.56	341.1	341.1, 324.3, 282.3, 206.1, 164.3, 136.3	P, U	-
M1	16.88	356.56	357.2	357.2, 340.2, 298.1, 207.0, 205.1, 164.2, 152.1	P, U, F	Hydroxylation or N/S Oxidation
M2	16.55	372.56	373.2	373.2, 355.3, 337.2, 331.3, 245.4, 227.1, 199.1, 159.3	P, U, F	Dihydroxylation
M3	16.45	326.56	326.3	326.3, 304.4, 191.1, 180.0, 136.2	F	O-Dealkylation
M4	15.99	516.56	516.3	516.3, 340.1, 312.1, 205.1, 136.3	P, U, F	O-Glucuronidation
M5	15.51	387.09	387.4	387.4, 347.3, 239.2, 197.2, 195.2, 177.1, 133.1	P, U	Hydroxylation+ S-Oxidation
M6	15.00	342.08	343.3	343.3, 327.4, 286.3, 197.3, 193.2, 166.2, 165.1, 149.2	P, U, F	Dealkylation+Hydroxylation
M7	11.52	502.56	503.0	503.0, 494.6, 481.1, 177.3, 133.1	F	O-Dealkylation+Glucuronidation

P: Plasma; U: Urine; F: Feces; Theoretical mass calculated for [M+H]

DISCUSSION

The current study offers a comprehensive assessment of 19-Monoaminothiazole (19MAT) through the amalgamation of bioanalytical technique validation, pharmacokinetic evaluation, and metabolic characterization, underpinned by *in silico* predictions and *in vivo* LC–MS/MS studies. These results provide whole picture of how compounds are absorbed, distributed, and metabolized, which is important for its development as a possible treatment. On a broader context, such triangulation of validated bioanalysis, PK, and metabolism is considered critical to derisk the scaffolds which are known to undergo a diverse oxidative and conjugative biotransformation specially thiazole-containing antivirals and similar heterocycles [41].

The LC–MS/MS method for measuring 19MAT was tested effectively to ensure its reliability and verify whether the same can be used repeatedly with the same results. Such validation is necessary to obtain reliable pharmacokinetic data, as any variation in matrix effects or assay performance may result in the misinterpretation of critical PK parameters. By meeting all the acceptance criteria of the regulatory guidelines, the validated method demonstrated a robust analytical framework that provided confidence in ensuring pharmacokinetic and metabolite profiling outcomes [31]. The method's applicability to different biological matrices facilitated extensive metabolic studies in plasma, urine, and feces. The comparable analytical approaches are routinely highlighted in recent work on thiazole-based medicinal chemistry and antiviral reports, where metabolite identification (e. g., O-dealkylation, S-oxidation) relying on sensitive, selective LC–MS/MS quantitation across various matrices [42].

As the primary objective of PK studies is rapid decision-making, not definitive statistical power, smaller sample size (n = 3) was used per dose group which is a standard practice during the early discovery evaluation as it offers the best balance between data reliability, resource use, and ethical considerations. While triplicate animals are acceptable for exploratory or preliminary PK assessments, the limited number reduces the statistical power and may not fully capture inter-individual variability. For future studies, larger cohorts can be used to strengthen the robustness of the findings.

The pharmacokinetic assessment of 19MAT demonstrated that 19MAT got rapidly absorbed into the systemic circulation, signifying advantageous permeability and effective uptake. The extended half-life of elimination shows that the drug is cleared slowly from the body, potentially as it spreads widely or might change into a different form. This data corresponds with the *in vitro* metabolic stability results, which also shown that 19MAT exhibits modest resistance to enzymatic degradation. This observation aligns with reports which concluded that thiazole derivatives exhibit favorable permeability, particularly when lipophilicity and polar surface area balance absorption along with distribution-based terminal phases. The data of *in vitro* metabolic stability shows that 19MAT exhibits modest resistance to enzymatic degradation, which was seen in related thiazole

scaffolds with variable microsomal stability, often improved by oxidations of metabolic sites identified *in silico* or via discovery metabolism screening experiments [42].

The oral bioavailability of about 23.82% is classified as moderate but acceptable for a new chemical entity, especially for compounds that are moderately lipophilic and have concerns about first-pass metabolism. The extensive metabolite formation observed in plasma, urine, and feces strongly supports hepatic and intestinal first-pass biotransformation as a major contributing factor for reduced systemic availability. Reviews of drug candidates with thiazole ring shown similarly observation about phase I oxidation and phase II conjugation can curtail bioavailability through dual-organ (liver/intestine) first-pass, reinforcing formulation or route-of-administration strategies to mitigate loss. The selected vehicle composition seems to enable efficient oral delivery, as indicated by quantifiable systemic exposure. The relatively low bioavailability, on the other hand, also makes it possible to investigate other ways to provide the drug, including sublingual or intramuscular delivery, which could avoid first-pass metabolic loss and possibly improve systemic uptake-an approach also reported in antiviral thiazole discovery where parenteral or alternate delivery is explored to bypass extensive first-pass metabolism [41, 42].

A clear variation was observed between the elimination half-life after intravenous administration ($t_{½}$ = 1.21 h) and after oral dosing ($t_{½}$ = 4.20 h). The longer apparent half-life in oral route, along with the prolonged mean residence time (MRTpo), suggests the possibility of flip-flop pharmacokinetics, wherein the rate of absorption becomes slower than the intrinsic elimination rate. Under such conditions, the terminal slope of the oral PK profile reflects absorption rather than elimination. Many heterocyclic drugs with moderate solubility, similar incidences of absorption-limited kinetics have been reported which can be sensitive to formulation and intestinal metabolism/transport, suggesting a multi-dose designs. This kinetic behavior is consistent with the compound's physicochemical characteristics and warrants further evaluation using multiple-dose or extended absorption models [42].

The estimated volume of distribution (~2 l/kg) indicates extensive tissue distribution beyond the vascular compartment. This characteristic may be advantageous for an antiviral compound, as it increases the chances of achieving therapeutically required concentrations within intracellular or tissue reservoirs where viral replication occurs. A larger V_d also support sustained exposure in target organs such as the lungs, spleen, lymphatic tissues, and other compartments relevant to viral dissemination. Comparable distributional behaviors have been noted for several thiazole-bearing therapeutics, where lipophilicity contributes to tissue partitioning, though high Vd which can complicate clearance predictions and frequency of dosing [42]. However, high tissue affinity may also influence clearance pathways and should be considered when designing dosing regimens.

The metabolic characterization of 19MAT unveiled a complicated biotransformation profile featuring seven major metabolites detected in plasma, urine, and feces. These metabolites arose via many pathways—hydroxylation, dealkylation, S-oxidation, and aromatic O-glucuronidation—demonstrating that 19MAT undergoes significant phase I and phase II enzymatic activities. Such metabolic pathways documented for thiazole and aminothiazole scaffolds, which frequently undergo ring-adjacent oxidation (including S-oxidation) and phenolic/aryl O-glucuronidation after O-dealkylation [43].

Aromatically coupled O-glucuronidation became a prominent phase II pathway, aligning with recognized metabolic trends for heterocyclic and aromatic amine-containing scaffolds. The lack of unmodified 19MAT in urine and feces indicates nearly full metabolic turnover, underscoring the importance of biotransformation in its elimination profile. This metabolic dominance elucidates the compound's extended half-life, as phase II processes frequently have varied enzymatic kinetics, potentially leading to delayed systemic clearance.

The *in vitro* metabolic investigation yielded only one mono-oxidized metabolite, suggesting possible discrepancies between microsomal enzyme activity and comprehensive *in vivo* metabolism. This difference shows that *in vitro* systems may not fully mimic all enzymatic pathways that are active in whole organisms. The difference in microsomal outcomes and *in vivo* complexity has been noted for aminothiazole-containing chemotypes, where extrahepatic enzymes, transporters, and co-factors involve metabolic routes beyond liver microsome predictions. This shows how important it is to use both methods to get an accurate picture of metabolism. It also suggests that the components of the formulation or physiological cofactors may affect metabolic sensitivity in living organisms [41, 43].

Enzymes present in the intestine, kidney, lungs, and plasma may contribute to oxidative and conjugative pathways that are not present in liver-only microsomal systems. The detection of several metabolites in feces samples suggests possible microbial involvement, since gut flora possesses reductases, hydrolases, and deconjugating enzymes capable of generating metabolite species absent in isolated microsomal incubations.

In silico metabolism profiling identified C15-located on the methoxy-substituted aromatic ring—as the principal site of metabolic liability, indicating that this position represents the dominant hotspot for biotransformation within the 19MAT scaffold. This prediction is strongly supported by the *in vivo* metabolite profile, where O-dealkylation of the methoxy group emerged as a prominent biotransformation pathway. The formation of the corresponding phenolic metabolite demonstrates that computational tools accurately anticipated the primary site of enzymatic reaction. This agreement shows that computer programs can be helpful in the early stages of medication research, especially when it comes to figuring out where metabolic hotspots are and how to analyze data. The overlap also shows how strong the LC–MS/MS procedure is in finding expected metabolites and confirming predicted pathways. Similar hotspot-guided design cycles have been applied to thiazole and aminothiazole drug candidates to mitigate reactive or labile positions (e. g., by blocking benzylic/methoxy sites or exchanging sulfur-containing rings to reduce bioactivation) [43].

Overall, the results show that 19MAT has a favorable pharmacokinetic and metabolic profile that could be used for further therapeutic testing. Because it is quickly absorbed, stays in the body for a long time, and has predictable metabolic pathways, it is a good candidate for more testing of antiviral action and mechanistic investigations. This positioning is consistent with the broader antiviral thiazole research, which identifies the scaffold as a productive source with drug-like properties when metabolism liabilities are understood and engineered. But the compound's vast metabolism suggests that future research should concentrate on; Comparative analysis of phase I and II pathways across species, with a focus on glucuronidation patterns, finding human-relevant metabolites, possibly through hepatocyte tests, alternative formulations or delivery routes to optimize systemic exposure, exploration of pharmacodynamic–pharmacokinetic relationships, especially if antiviral potency is demonstrated and investigation of potential CYP450 inhibition or induction by 19MAT for understanding of metabolic profile. These next steps are aimed at balancing efficacy with metabolic safety and avoiding reactive intermediate liabilities in thiazole medicinal chemistry and metabolism.

Such investigations will be essential for determining the translational potential of 19MAT and ensuring that its metabolic characteristics support safe and effective therapeutic use. The lessons learned from earlier thiazole-based antivirals and drug leads—regarding absorption limits, bioactivation risks, and conjugation-driven clearance—provide a clear roadmap for taking the research work of 19MAT, forward.

CONCLUSION

This integrated *in silico* and *in vivo* study successfully developed and validated a robust LC–MS/MS bioanalytical technique for the quantitative analysis of 19MAT in biological matrices. The approach showed very good accuracy, precision, recovery, and matrix stability, which showed that it was good for pharmacokinetic and metabolic research. With this validated platform, the pharmacokinetic profile of 19MAT showed that it was

quickly absorbed into the body, had a long elimination half-life, and had moderate oral bioavailability. This means that the chosen formulation worked well to allow systemic exposure.

A thorough analysis of metabolites in plasma, urine, and feces revealed seven main metabolites. Hydroxylation, dealkylation, S-oxidation, and aromatic O-glucuronidation were found to be the main metabolic processes. The lack of the parent chemical in excreta indicates significant biotransformation, corroborated by both *in silico* predictions and *in vivo* observations. *In vitro* metabolism tests revealed only one mono-oxidized product; however, the overall results emphasize the necessity for a more comprehensive examination of phase I and phase II pathways across several species, including humans.

This correlative technique provides a fundamental comprehension of the bioanalytical performance, pharmacokinetics, and metabolic disposition of 19MAT. These results furnish a robust foundation for propelling the chemical into more antiviral assessment, mechanistic *in vitro* characterization, and forthcoming translational investigations.

ACKNOWLEDGEMENT

The author is thankful to Dr. Venkatesan Jayaprakash for helping with this research by providing the test compound. During initial drafting, the author(s) used AI tool [Copilot AI tool]. After using this tool, the authors reviewed and edited the content as needed and took full responsibility for the content of the publication.

FUNDING

This work did not receive any financial support.

AUTHORS CONTRIBUTIONS

Vinay N. Basavanakatti: Methodology, Investigation, Software, Writing original draft; Mohammad Ali: Conceptualization, Visualization, Resources, Supervision, Project administration, Validation, Writing, review, and editing; Sheikh Murtuja: Data curation, Formal analysis, Software, Writing, review, and editing; Barij Nayan Sinha: Data curation, Formal analysis, Software, Validation, Writing, review, and editing; Venkatesan Jayaprakash: Data curation, Formal analysis, Validation, Writing, review, and editing.

CONFLICT OF INTERESTS

The authors declare no competing interests.

REFERENCES

1. Prakash C, Shaffer CL, Nedderman A. Analytical strategies for identifying drug metabolites. Mass Spectrom Rev. 2007;26(3):340-69. doi: 10.1002/mas.20128, PMID 17405144.
2. Wang J, Urban L. The impact of early ADME profiling on drug discovery and development strategy. Drug Discov Today. 2004;5:73-86.
3. Want EJ, Compton BJ, Hollenbeck T, Siuzdak G. The application of mass spectrometry in pharmacokinetics studies. J Spectrosc. 2003;17(4):681-91. doi: 10.1155/2003/369786.
4. Doğan HO. Metabolomics: a review of liquid chromatography mass spectrometry-based methods and clinical applications. Turk J Biochem. 2024;49(1):1-14. doi: 10.1515/tjb-2023-0095.
5. Zhou B, Xiao JF, Tuli L, Ressom HW. LC-MS-based metabolomics. Mol Biosyst. 2012;8(2):470-81. doi: 10.1039/c1mb05350g, PMID 22041788.
6. Shah P, Shah J, Saroj S, Jairaj V, Rathod R. Metabolite identification by mass spectrometry. Int J Pharm Res Allied Sci. 2015;4:9-17.
7. Sowjanya G, Ganapaty S, Sharma R. *In vitro* test methods for metabolite identification: a review. Asian J Pharm Pharmacol. 2019;5(3):441-50. doi: 10.31024/ajpp.2019.5.3.2.
8. Theodoridis G, Gika HG, Wilson ID. LC-MS-based methodology for global metabolite profiling in metabonomics/metabolomics. TrAC Trends Anal Chem. 2008;27(3):251-60. doi: 10.1016/j.trac.2008.01.008.
9. Lee JY, Kim SK, Lee K, Oh SJ. The Application of mass spectrometry in Drug Metabolism and Pharmacokinetics. Adv Exp Med Biol. 2021;1310:533-50. doi: 10.1007/978-981-33-6064-8_20, PMID 33834449.
10. Prakash C, Soliman V. Metabolism and excretion of a novel antianxiety drug candidate, CP-93,393, in Long Evans rats. Differentiation of regioisomeric glucuronides by LC/MS/MS. Drug Metab Dispos. 1997;25(11):1288-97. PMID 9351906.
11. Rincon Nigro ME, Du T, Gao S, Kaur M, Xie H, Olaleye OA et al. Metabolite identification of a novel anti-leishmanial agent OJT007 in rat liver microsomes using LC-MS/MS. Molecules. 2022;27(9):2854. doi: 10.3390/molecules27092854, PMID 35566205.
12. Howlader S, Kim MJ, Jony MR, Long NP, Cho YS, Kim DH et al. Characterization of clofazimine metabolism in human liver microsomal incubation *in vitro*. Antimicrob Agents Chemother. 2022;66(10):e0056522. doi: 10.1128/aac.00565-22, PMID 36190267.
13. Al-Shakliah NS, Attwa MW, AlRabiah H, Kadi AA. Identification and characterization of *in vitro*, *in vivo*, and reactive metabolites of tandutinib using liquid chromatography ion trap mass spectrometry. Anal Methods. 2021;13(3):399-410. doi: 10.1039/d0ay02106g, PMID 33410830.
14. Guo J, Zhang M, Elmore CS, Vishwanathan K. An integrated strategy for *in vivo* metabolite profiling using high-resolution mass spectrometry based data processing techniques. Anal Chim Acta. 2013;780:55-64. doi: 10.1016/j.aca.2013.04.012, PMID 23680551.
15. Xi R, Abdulla R, Zhao J, Aisa HA, Liu Y. Pharmacokinetic study and metabolite identification of CAM106 in rats by validated UHPLC-MS/MS. Pharmaceuticals (Basel). 2023;16(5):728. doi: 10.3390/ph16050728, PMID 37242511.
16. Attwa MW, Kadi AA, Darwish HW, Amer SM, Al-Shakliah NS. Identification and characterization of *in vivo*, *in vitro* and reactive metabolites of vandetanib using LC–ESI–MS/MS. Chem Cent J. 2018;12(1):99. doi: 10.1186/s13065-018-0467-5, PMID 30251155.
17. Forkuo AD, Ansah C, Pearson D, Gertsch W, Cirello A, Amaral A, et al. Identification of cryptolepine metabolites in rat and human hepatocytes and metabolism and pharmacokinetics of cryptolepine in Sprague Dawley rats. BMC Pharmacol Toxicol. 2017;18(1):84. doi: 10.1186/s40360-017-0188-8, PMID 29273084.
18. Dwivedi MK, Sonter S, Mishra S, Singh P, Singh PK. Secondary metabolite profiling and characterization of diterpenes and flavones from the methanolic extract of Andrographis paniculata using HPLC–LC–MS/MS. Future J Pharm Sci. 2021;7(1):188. doi: 10.1186/s43094-021-00292-6.
19. Hu T, Ge X, Wang J, Zhang N, Diao X, Hu L et al. Metabolite identification of iridin in rats by using UHPLC-MS/MS and pharmacokinetic study of its metabolite irigenin. J Chromatogr B Analyt Technol Biomed Life Sci. 2021;1181:122914. doi: 10.1016/j.jchromb.2021.122914, PMID 34492510.
20. Shi X, Liu M, Zhang M, Zhang K, Liu S, Qiao S, et al. Identification of *in vitro* and *in vivo* metabolites of isoimperatorin using liquid chromatography/mass spectrometry. Food Chem. 2013;141(1):357-65. doi: 10.1016/j.foodchem.2013.02.068, PMID 23768368. foodchem.2013.02.068.

21. Su H, Boulton DW, Barros A, Wang L, Cao K, Bonacorsi SJ, et al. Characterization of the *in vitro* and *in vivo* metabolism and disposition and cytochrome P450 inhibition/induction profile of saxagliptin in human. Drug Metab Dispos. 2012;40(7):1345-56. doi: 10.1124/dmd.112.045450, PMID 22496391.
22. Yang S, Shi W, Hu D, Zhang S, Zhang H, Wang Z, et al. *In vitro* and *in vivo* metabolite profiling of valnemulin using ultraperformance liquid chromatography-quadrupole/time-of-flight hybrid mass spectrometry. J Agric Food Chem. 2014;62(37):9201-10. doi: 10.1021/jf5012402, PMID 25156794.
23. Yu L, Chen X, Zhang WS, Zheng L, Xu WW, Xu MY, et al. Metabolite identification, tissue distribution, excretion and preclinical pharmacokinetic studies of ET-26-HCl, a new analogue of etomidate. R Soc Open Sci. 2020;7(2):191666. doi: 10.1098/rsos.191666, PMID 32257329.
24. Thakkar D, Kate AS. In silico, *in vitro* and *in vivo* metabolite identification of brexpiprazole using ultra-high-performance liquid chromatography/quadrupole time-of-flight mass spectrometry. Rapid Commun Mass Spectrom. 2019;33(11):1024-35. doi: 10.1002/rcm.8436, PMID 30889624.
25. Jia Z, Qiu Q, He R, Zhou T, Chen L. Identification of metabolite interference is necessary for accurate LC-MS targeted metabolomics analysis. Anal Chem. 2023;95(20):7985-92. doi: 10.1021/acs.analchem.3c00804. PMID 37155916.
26. Alseekh S, Aharoni A, Brotman Y, Contrepois K, D'Auria J, Ewald J, et al. Mass spectrometry-based metabolomics: a guide for annotation, quantification and best reporting practices. Nat Methods. 2021;18(7):747-56. doi: 10.1038/s41592-021-01197-1, PMID 34239102.
27. Xiao JF, Zhou B, Ressom HW. Metabolite identification and quantitation in LC–MS/MS-based metabolomics. Trends Analyt Chem. 2012;32:1-14. doi: 10.1016/j.trac.2011.08.009. PMID 22345829.
28. Griffiths WJ, Koal T, Wang Y, Kohl M, Enot DP, Deigner HP. Targeted metabolomics for biomarker discovery. Angew Chem Int Ed Engl. 2010;49(32):5426-45. doi: 10.1002/anie.200905579, PMID 20629054.
29. Saito K, Matsuda F. Metabolomics for functional genomics, systems biology, and biotechnology. Annu Rev Plant Biol. 2010;61:463-89. doi: 10.1146/annurev.arplant.043008.092035. PMID 19152489.
30. Oliver SG, Winson MK, Kell DB, Baganz F. Systematic functional analysis of the yeast genome. Trends Biotechnol. 1998;16(9):373-8. doi: 10.1016/S0167-7799(98)01214-1, PMID 9744112.
31. Basavanakatti VN, Ali M, Bharathi DR, Murtuja S, Sinha BN, Jayaprakash V, et al. Development and validation of HPLC-UV and LC-MS/MS methods for the quantitative determination of a novel aminothiazole in preclinical samples. BMC Chem. 2024;18(1):220. doi: 10.1186/s13065-024-01321-0, PMID 39511665.
32. US Food and Drug Administration. Bioanalytical method validation—guidance for industry. In: https://www. fda. gov/files/drugs/published/Bioanalytical-Method-Validation-Guidance-for-Industry. pdf; 2018. Available.
33. International Council for Harmonisation (ICH), "ICH guideline M10 on bioanalytical method validation and study sample analysis. EMA/CHMP/ICH/172948/2019; May 24 2022.
34. BioTransformer 3.0. [cited 2026 Mar 20]. Available from: https://biotransformer. ca.
35. Yu JC, Martin S, Nasr J, Stafford K, Thompson D, Petrikovics I. LC-MS/MS analysis of 2-aminothiazoline-4-carboxylic acid as a forensic biomarker for cyanide poisoning. World J Methodol. 2012;2(5):33-41. doi: 10.5662/wjm.v2.i5.33, PMID 25237615.
36. Gurav P, Damle M. Bioanalytical method for estimation of teriflunomide in human plasma. Int J Pharm Pharm Sci. 2022;14(9):19-23. doi: 10.22159/ijpps.2022v14i9.45151.
37. Olsen L, Montefiori M, Tran KP, Jørgensen FS. SMARTCyp 3.0: enhanced cytochrome P450 site-of-metabolism prediction server. Bioinformatics. 2019;35(17):3174-5. doi: 10.1093/bioinformatics/btz037, PMID 30657882.
38. Rydberg P, Gloriam DE, Zaretzki J, Breneman C, Olsen L. SMARTCyp: A 2D method for prediction of cytochrome P450-mediated drug metabolism. ACS Med Chem Lett. 2010;1(3):96-100. doi: 10.1021/ml100016x, PMID 24936230.
39. Rydberg P, Gloriam DE, Olsen L. The SMARTCyp cytochrome P450 metabolism prediction server. Bioinformatics. 2010;26(23):2988-9. doi: 10.1093/bioinformatics/btq584, PMID 20947523.
40. Bapiro TE, Martin S, Wilkinson SD, Orton AL, Hariparsad N, Harlfinger S et al. The disconnect in intrinsic clearance determined in human hepatocytes and liver microsomes results from divergent cytochrome P450 activities. Drug Metab Dispos. 2023;51(7):892-901. doi: 10.1124/dmd.123.001323, PMID 37041083.
41. Singh IP, Gupta S, Kumar S. Thiazole compounds as antiviral agents: an update. Med Chem. 2020;16(1):4-23. doi: 10.2174/1573406415666190614101253, PMID 31203807.
42. Petrou A, Fesatidou M, Geronikaki A. Thiazole ring-A biologically active scaffold. Molecules. 2021 May 25;26(11):3166. doi: 10.3390/molecules26113166, PMID 34070661, PMCID PMC8198555.
43. Jaladanki CK, Khatun S, Gohlke H, Bharatam PV. Reactive metabolites from thiazole-containing drugs: quantum chemical insights into biotransformation and toxicity. Chem Res Toxicol. 2021 Jun 21;34(6):1503-17. doi: 10.1021/acs.chemrestox.0c00450 [ePub]. PMID 33900062.